Available online at www.sciencedirect.com
ScienceDirect
Journal of Catalysis 251 (2007) 28–38
JOURNAL OF CATALYSIS
www.elsevier.com/locate/jcat

The fate of platinum in $Pt/Ba/CeO_2$ and $Pt/Ba/Al_2O_3$ catalysts during thermal aging

Maria Casapu [a], Jan-Dierk Grunwaldt [a,*], Marek Maciejewski [a], Alfons Baiker [a,*], Stephan Eckhoff [b], Ulrich Göbel [b], Meike Wittrock [b]

[a] *Institute for Chemical and Bioengineering, Department of Chemistry and Applied Biosciences, ETH Zurich, Hönggerberg, HCI, CH-8093 Zurich, Switzerland*
[b] *Umicore AG & Co. KG, Rodenbacher Chaussee 4, D-63403 Hanau-Wolfgang, Germany*

Received 6 June 2007; revised 17 July 2007; accepted 18 July 2007

Available online 30 August 2007

Abstract

The behavior of Pt during aging of $Pt/Ba/CeO_2$ and $Pt/Ba/Al_2O_3$ NO_x storage-reduction catalysts (NSR) was studied using model catalysts with high and low Pt loadings. Pt composite formation, due to the possible reaction between BaO and platinum oxides, was observed in several cases and was elucidated by a series of analytical techniques, including X-ray diffraction (XRD), thermal analysis (TA), X-ray absorption spectroscopy (XANES, EXAFS), and electron microscopy. During calcination of mechanical mixtures of $BaCO_3$ and PtO_2, $BaPtO_3$ was formed at ca. 600 °C, transforming to $BaPtO_{2.38}$ above 800 °C. Investigation of $Pt/Ba/CeO_2$ and $Pt/Ba/Al_2O_3$ model catalysts with high and low Pt loadings revealed that in the case of $Pt/Ba/CeO_2$, the mixed oxide $BaPtO_3$ was formed at relatively low temperature (600–700 °C) in oxidizing atmosphere. Above 800 °C, $BaPtO_3$ reacted further with $BaCeO_3$ to form a double perovskite, Ba_2PtCeO_6. In contrast, for $Pt/Ba/Al_2O_3$, only the sintering of Pt, with no mixed Pt–Ba oxides, was found. The recovery of the catalytically active metallic Pt species could be achieved in the aged $Pt/Ba/CeO_2$ catalyst by reduction with hydrogen at relatively low temperature. Finally, investigation of the NO_x storage and reduction activity of the fresh, aged, and reduced catalyst confirmed that this treatment is beneficial for catalyst reactivation.

Keywords: NO_x storage-reduction catalysts; Aging; Platinum composites; $BaPtO_3$; Ba_2PtCeO_6; Reactivation; Thermal analysis; X-ray absorption spectroscopy

1. Introduction

The introduction of lean-burn engines with direct fuel injection is presently one of the most promising concepts for decreasing fuel consumption and thereby reducing associated CO_2 emissions [1,2]. However, neither the conventional oxidation catalysts nor three-way catalysts are able to reduce NO_x emissions under lean conditions. The most promising strategy for reducing NO_x emissions is to use the NO_x storage-reduction (NSR) catalyst [1,3,4]. The NSR catalysts normally contain noble metals (Pt, Rh) for the oxidation of NO to NO_2 (under lean fuel conditions) and the reduction of stored NO_x (under rich conditions), and a storage component deposited on carrier oxides with a high surface area, such as La_2O_3-stabilized γ-Al_2O_3 or CeO_2 [3–6]. The NSR performance of such catalysts depends on various factors, including the dispersion of the noble metal and the Ba constituent as well as its thermal stability, structural and textural properties. Deactivation of NSR catalysts is caused mainly by sulfur and thermal deterioration. Apart from the development of catalysts with higher tolerance for SO_2 or SO_2-derived species [7], one of the major challenges is therefore the improvement of the thermal stability and the development of possible reactivation procedures.

Generally, thermal deterioration induces sintering of catalytically active phases, the collapse of the pore structure of the support, and chemical transformations of catalytically active species, for example, during their reaction with the support. For automotive catalysts, the reaction of the catalytic phase with the support or other washcoat components [8,9], particle growth of the precious metals [10,11], sintering of the support and encapsulation of active metal particles [12,13], and

* Corresponding authors.
E-mail addresses: grunwaldt@chem.ethz.ch (J.-D. Grunwaldt), baiker@chem.ethz.ch (A. Baiker).

0021-9517/$ – see front matter
doi:10.1016/j.jcat.2007.07.019

volatilization of active compounds [14] have been encountered. In addition, several studies of NO_x storage-reduction catalysts have been reported; these have focused on the formation of Ba-support composite oxides and sintering of noble metal particles [5,8,9,15]. Also important is encapsulation of the noble metals by reducible supports and formation of rhodium aluminates [16,17]. Surprisingly little attention has been given to the possible reaction between BaO and the platinum constituent, both of which are present in NSR catalysts. Despite its relative chemical inertness and stability, platinum reacts at high temperatures with alkali and alkaline earth metal to form mixed oxides. The reaction between $BaCO_3$ and PtO_2 or Pt black in oxidizing environments above 800 °C has been reported [18–21]. The products of this reaction are $BaPtO_3$ [19,21], Ba_4PtO_6 [18], and $Ba_3Pt_2O_7$, a solid solution with general formula $Ba_3Pt^{4+}_{2+x}O_{7+2x}$ [22,23]. Using diffraction and anomalous fine-structure data, Vacinova and Hodeau [24] recently showed that the solid solution can be generally better described by the formula $Ba_p(Ba_xPt^{2+}_{1-x})Pt^{4+}_{p-2}O_{3p-3}$, where p represents oxygen deficiency and x is a possible substitution of Pt^{2+} by Ba^{2+}.

Platinum plays a double role in a NO_x storage-reduction cycle in the oxidation of NO to NO_2 (initiation of the storage process) and in regeneration, consisting of reduction of the stored NO_x species by H_2, CO, and hydrocarbons. Thus, the loss of Pt through the reaction with BaO could significantly affect the overall NO_x storage-reduction activity. Taking this scenario into account, in the present work we focused on the possible reaction between Pt- and Ba-containing species in $Pt/Ba/CeO_2$ and $Pt/Ba/Al_2O_3$ catalysts. For this purpose, we first investigated the processes occurring during calcination of $BaCO_3$ and PtO_2 mechanical mixtures and $Pt/Ba/CeO_2$ and $Pt/Ba/Al_2O_3$ model catalysts with high Pt loading, then studied the fate of Pt in model catalysts with low Pt loading, which have a greater practical relevance. Finally, we evaluated possible strategies for the reactivation of aged $Pt/Ba/CeO_2$ catalysts.

2. Experimental

2.1. Sample preparation

2.1.1. Preparation of model Ba–Pt oxides using the mechanical mixture of $BaCO_3$ and PtO_2

Two series of model samples were prepared using the mechanical mixing of $BaCO_3$ (Fluka) and PtO_2 (Aldrich) in molar ratios of 4:1 and 1:1. These ratios were selected to be in the stoichiometric range required for the synthesis of all Ba–Pt mixed oxides that could be formed. The samples were calcined in a furnace (Nabertherm) in air for 12 h at 600, 700, 800, 900, and 1000 °C.

2.1.2. Aged $Pt/Ba/\gamma\text{-}Al_2O_3$ and $Pt/Ba/CeO_2$ catalysts

These catalysts were prepared by incipient wetness impregnation of the commercial γ-alumina and ceria (Umicore) supports with aqueous solutions of dinitrodiamine platinum (Strem Chemicals) and barium acetate (Fluka) as described previously [8]. To monitor the reaction between Pt and the other components in the system with different analytical methods, two types of impregnated model catalysts were prepared: high-loaded Pt(10 g)/Ba(20 g)/support(100 g), designated 10-Pt/Ba/support, and low-loaded Pt(1 g)/Ba(20 g)/support(100 g), designated 1-Pt/Ba/support. Aging was done by calcination of the raw catalysts for 12 h in air in a furnace (Nabertherm) at 600, 700, 800, 900 and 1000 °C, if not stated otherwise in the text.

2.2. Characterization techniques

2.2.1. X-ray diffraction

X-ray diffraction measurements were carried out on a Siemens D5000 powder X-ray diffractometer using the CuK_α radiation in the step scanning mode between $2\theta = 15$ and 65°, with a step size of 0.01° and 2 s per step. The pattern intensities were standardized by comparison with the inert standard, i.e. the intensity of Cu(111) reflection at $2\theta = 43.178°$.

2.2.2. Thermal analysis

Thermal analysis (TA and PulseTA [25]) experiments were performed on a Netzsch STA 409 thermoanalyzer equipped with a pulse device enabling injection of a certain amount of one or two pure gases or gaseous mixtures into the carrier gas stream flowing through the system. The flow rate was controlled by mass flow controllers (Brooks model 5850E). The outlet of the thermoanalyzer was connected by a heated (ca. 150 °C) stainless steel capillary to a mass spectrometer (Pfeiffer Vacuum OmniStar). Typically, a 70-mg powdered sample was used, and the heating ramp rate was 10 °C/min.

2.2.3. XANES and EXAFS experiments

These experiments were performed at the beamline X1 at HASYLAB, Hamburg, Germany. The storage ring typically operates at 4.45 GeV with an injection current of 140 mA. A Si(111) double-crystal was used as monochromator. The higher harmonics were removed by detuning the crystals to 60% of the maximum intensity. EXAFS data were collected in the fluorescence and transmission mode. A five-element Ge solid-state detector was used to measure the fluorescence X-rays of the element of interest. Spectra were obtained around the Pt L_3-edge (11.564 keV), using Pt foil as reference for energy calibration.

Additional measurements at the Pt L_3-edge were performed at the Swiss–Norwegian beamline (SNBL) at the European Synchrotron Radiation Facility (ESRF) in Grenoble, France. The electron energy was 6.0 GeV, and the maximum ring current was 200 mA. A Si(111) crystal was used as a monochromator. EXAFS data were collected in the fluorescence and transmission modes at room temperature with varying temperature and gas compositions [26].

The in situ XANES and EXAFS experiments were done at the Swiss–Norwegian beamline (SNBL) at the European Synchrotron Radiation Facility (ESRF) in Grenoble using an in situ cell with X-ray fluorescence and transmitting windows. The sample was placed in a 45° angle to both the beam and the detector. The temperature in the system was increased up to

500 °C at a rate of 5 °C/min. Experiments were carried out in the atmosphere of 5 vol% H_2/balance He. The outlet of the cell was connected to a mass spectrometer (Pfeiffer Vacuum OmniStar). WINXAS 3.1 software was used for data evaluation [27]. Fourier transformation of the EXAFS data was applied on the k^3-weighted $\chi(k)$ data.

2.2.4. Electron microscopy

The transmission electron microscopy (TEM), scanning transmission electron microscopy (STEM) and energy-dispersive X-ray (EDX) investigations were performed on a Tecnai F30 microscope. Crushed samples were suspended in ethanol and deposited on a holey carbon foil supported on a copper grid. TEM images were recorded with a slow-scan CCD camera. The EDX spectrometer (EDAX) attached to the Tecnai F30 allows investigators to perform elemental analyses at spots selected in the HAADF-STEM images.

3. Results

3.1. Reaction between $BaCO_3$ and PtO_2

To investigate the reactions occurring during the calcination in the $BaCO_3$–PtO_2 system, the mechanical mixtures of $BaCO_3$:PtO_2 (molar ratios 4:1 and 1:1) were heated in the thermoanalyzer in an inert (He) and oxidizing atmospheres (10% O_2/He) at a rate of 5 °C/min from room temperature to ca. 1250 °C. The thermogravimetric (TG) and differential thermogravimetric (DTG) curves recorded during heating in 10% O_2/He atmosphere are depicted in Figs. 1a and 1c. The decomposition of bulk $BaCO_3$ in an inert atmosphere occurred in the range of 800–1400 °C with a maximum of the CO_2 evolution at 1100 °C [28]. The TG and DTG curves and the mass spectrometric signals of CO_2 ($m/z = 44$) show that onset of the decomposition of $BaCO_3$ in the presence of PtO_2 shifted to lower temperature (about 600 °C) due to the formation of Pt–Ba oxides. $BaCO_3$ disappeared faster in the system containing more PtO_2 (1:1 ratio instead of 1:4 ratio of PtO_2 and $BaCO_3$). The XRD patterns of the samples obtained at selected temperatures (marked on the TG curve in Figs. 1a and 1c) indicate a similar stoichiometry of the solid-state reactions in the 1:1 and 4:1 systems—more specifically, formation of $BaPtO_3$ in a first step. Note that metallic platinum also was observed above 600 °C (Figs. 1b and 1d), at a temperature at which bulk PtO_2 decomposes in 10% O_2/He (as indicated by the MS signal of O_2, $m/z = 32$, in Figs. 1a and 1c).

Further temperature increases led to decomposition of $BaPtO_3$ and formation of oxygen-deficient oxides with general formula $BaPtO_{3-x}$, as reported previously [21]. At around 800 °C, the characteristic XRD patterns of $BaPtO_{2.38}$ could be

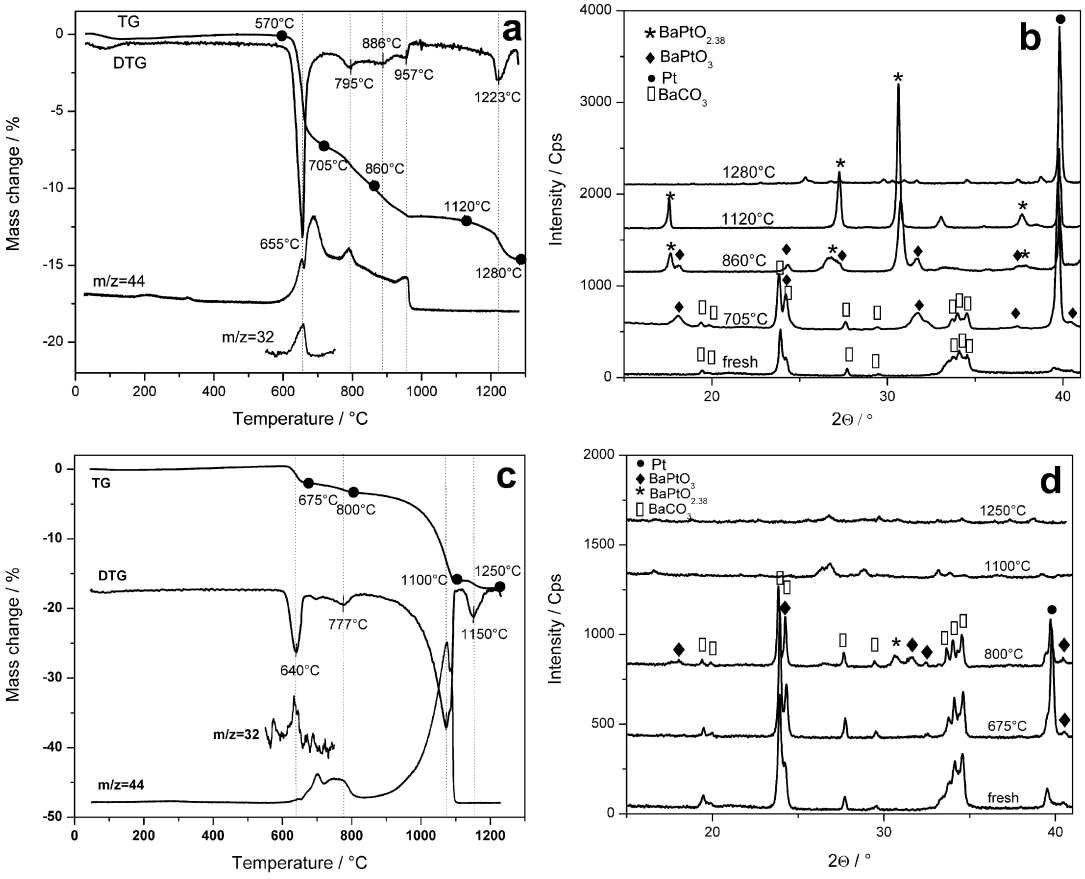

Fig. 1. TG and DTG signals of the mechanical mixtures of $BaCO_3$:PtO_2 in a ratio 1:1 (a) and 4:1 (c) and the corresponding XRD patterns (b) and (d). TA was conducted during heating in 10% O_2/He with a rate of 5 °C/min (note that the evolution of oxygen due to PtO_2 decomposition is visible between 500 and 800 °C despite the oxygen atmosphere); XRD patterns were recorded after TA experiments stopped at temperatures marked on the TG curve in (a) and (c).

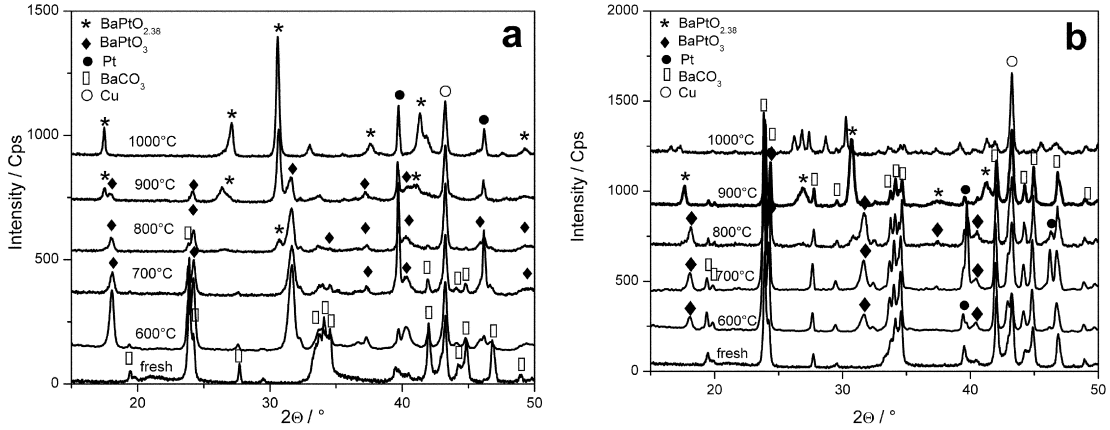

Fig. 2. XRD patterns of the mechanical mixtures of $BaCO_3$:PtO_2 in a ratio of 1:1 (a) and 4:1 (b) calcined at different temperatures for 12 h. The samples synthesized at 600 °C were calcined for one week.

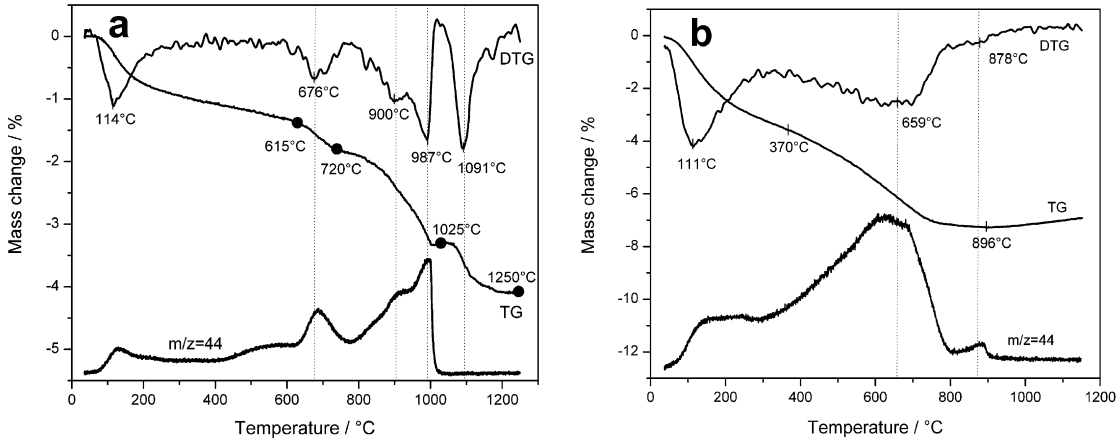

Fig. 3. TG, DTG and mass spectrometric signal of $m/z = 44$ recorded during calcination of 10-Pt/Ba/CeO_2 (a) and of 10-Pt/Ba/Al_2O_3 (b) in 10%O_2/He with a rate of 5 °C/min.

identified. Above 1120 °C, this mixed oxide lost more oxygen, giving phases with unknown stoichiometric composition. These conditions are beyond those encountered during the application of NO_x storage-reduction catalysts, however.

The formation of Ba–Pt mixed oxides was not detected by XRD measurements if the calcination of $BaCO_3$–PtO_2 mixtures was done in an inert atmosphere. In this atmosphere, PtO_2 already starts to decompose at about 475 °C, too low for the formation of Ba–Pt oxides.

To achieve a more complete understanding of the formation of Ba–Pt mixed-oxide phases as a function of temperature and of the Ba:Pt ratio, the two mechanical mixtures were calcined in air at selected temperatures between 600 and 1000 °C. The corresponding XRD patterns are depicted in Figs. 2a and 2b. In both cases, the first phase, observed already at 600 °C after 1 week of calcination, was $BaPtO_3$. At this temperature, the characteristic patterns of metallic Pt were also present. At 800 °C, both $BaPtO_3$ and $BaPtO_{2.38}$ were observed. At 900 °C, the 1:1 system contained both oxides, whereas in the 4:1 system, only $BaPtO_{2.38}$ was present, and all metallic Pt had been consumed. The formation of a new, unknown Ba–Pt oxide was detected at 1000 °C in the Ba-rich system, and the presence of $BaPtO_{2.38}$ and metallic Pt were detected in the 1:1 system.

3.2. The reaction between Pt and the other components in Pt/Ba/CeO_2 and Pt/Ba/Al_2O_3 catalysts

The formation of Ba–Pt oxides in NO_x storage catalysts can lead to a loss of the noble metal activity, which in turn may affect various important steps, such as hydrogen activation, NO oxidation, and the cracking of hydrocarbons. Consequently, this potential reaction of platinum was investigated in Pt/Ba/CeO_2 and Pt/Ba/Al_2O_3 samples using different analytical methods. XRD, thermal analysis, and mass spectrometry were applied for the high-loading samples (10-Pt/Ba/CeO_2 and 10-Pt/Ba/Al_2O_3), and X-ray absorption spectroscopy and electron microscopy were used for the low-loading samples (1-Pt/Ba/CeO_2 and 1-Pt/Ba/Al_2O_3).

3.2.1. High-loading sample 10-Pt/Ba/CeO_2

The sample was at first calcined in the thermoanalyzer under oxidizing atmosphere in 10% O_2/He with 10 °C/min up to 1300 °C. The TG and DTG curves, together with the MS signals of O_2 and CO_2 recorded during calcination, are shown in Fig. 3a. Whereas for this high-loaded sample, CO_2 evolution originating from $BaCO_3$ decomposition was already observed at 450 °C (Fig. 3a), in the corresponding Pt-free Ba/CeO_2 sam-

ple, $BaCO_3$ began to decompose at about 750 °C (not shown). The peak centered at 676 °C corresponded to the reaction of amorphous $BaCO_3$ with PtO_2 and formation of $BaPtO_3$. This transformation was confirmed by the XRD measurements of the sample calcined in 10% O_2/He in the thermoanalyzer up to 720 °C (Fig. 4). A second region of CO_2 evolution started above 770 °C when the Ba–Pt–Ce mixed oxide was formed and characteristic XRD reflections of Ba_2CePtO_6 were present in XRD patterns of the sample calcined up to 1025 °C (Fig. 4).

The formation of Ba_2CePtO_6 was also reported by Ouchetto et al. [29] during synthesis of bariumcuprocerates in Pt crucibles. According to Ouchetto, Ba_2CePtO_6 is formed in the reaction between synthesized $BaCeO_3$ and Pt and O_2 from air. In our study, we noted a different pathway of Ba_2CePtO_6 formation. The XRD patterns shown in Fig. 4 reveal the consecutive steps of this process. Around 670 °C, PtO_2 partly reacted with BaO to form $BaPtO_3$ (with the rest decomposed to Pt and O_2). Further temperature increases led to the formation of $BaCeO_3$ due to the reaction between CeO_2 and BaO and/or $BaCO_3$. Immediately after synthesis, the freshly formed $BaCeO_3$ reacted with $BaPtO_3$ to Ba_2CePtO_6. This scenario also may explain the absence of the XRD patterns characteristic for $BaCeO_3$ that we observed previously at 800–1000 °C [8]. At 1050 °C Ba_2CePtO_6 started to decompose to $BaCeO_3$ and Pt (Figs. 3 and 4).

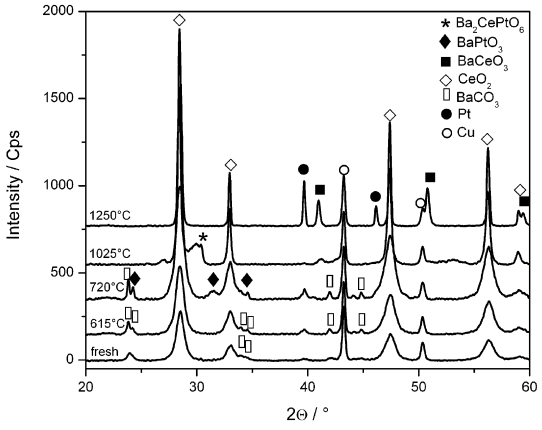

Fig. 4. XRD patterns of the 10-Pt/Ba/CeO_2 sample after TA analysis stopped at temperatures marked on the TG curve in Fig. 3a.

To complete the investigation into the course of the solid-state reactions occurring in the system, the 10-Pt/Ba/CeO_2 sample was calcined in air at different temperatures between 700 and 1000 °C. The XRD patterns obtained after calcination are depicted in Fig. 5a. The formation of $BaPtO_3$ was observed at 700 °C. $BaCeO_3$ formed at 800 °C [8] reacted with $BaPtO_3$, giving Ba_2CePtO_6. Traces of $BaPtO_3$ remained visible in the XRD patterns even at 1000 °C.

3.2.2. *High-loading sample 10-Pt/Ba/Al_2O_3*

The TG, DTG, and MS signals recorded during calcination of 10-Pt/Ba/Al_2O_3 in 10% O_2 are depicted in Fig. 3b. The evolution of CO_2 (mass spectrometric signal $m/z = 44$) indicates that the decomposition of $BaCO_3$ started at 300 °C. This low-temperature decomposition of $BaCO_3$ is due to the high dispersion of $BaCO_3$ on Al_2O_3 [30]. Compared with the CeO_2-supported sample, the presence of Pt had no significant influence on the decomposition of Al_2O_3-supported $BaCO_3$. The XRD measurements performed with 10-Pt/Ba/Al_2O_3 after calcination in 10% O_2/He up to certain temperatures (marked on the TG curve in Fig. 3b) revealed only sintering of Pt and formation of $BaAl_2O_4$ at higher temperature. The results of additional XRD investigations of the sample calcined at different temperatures between 700 and 1000 °C are shown in Fig. 5b. In contrast to the $BaCO_3$–PtO_2 mechanical mixtures, and the 10-Pt/Ba/CeO_2 catalyst, the formation of Ba–Pt oxides was not observed in this system.

This surprisingly different behavior could be caused by an intimate contact resulting in a strong interaction between Ba-containing species and Al_2O_3 in this catalyst. In fact, it has been reported that Ba compounds can stabilize the surface area and suppress phase transformation of γ-Al_2O_3 by formation of –Ba–O–Al– surface bonds [31–33]. Our previous studies showed that the surface area of a Pt(0.84 wt%)/Ba(16.7%)/Al_2O_3 model catalyst decreased from 128 m^2/g (after preparation) to 89 m^2/g after calcination at 1100 °C for 10 h. In contrast, for the Pt(0.84 wt%)/Ba(16.7%)/CeO_2 catalyst, we observed a much stronger surface area decrease after calcination at 1000 °C for 10 h [8]. The significant sintering of Pt observed on the alumina supported catalyst is in very good agreement with results of previous studies [34,35].

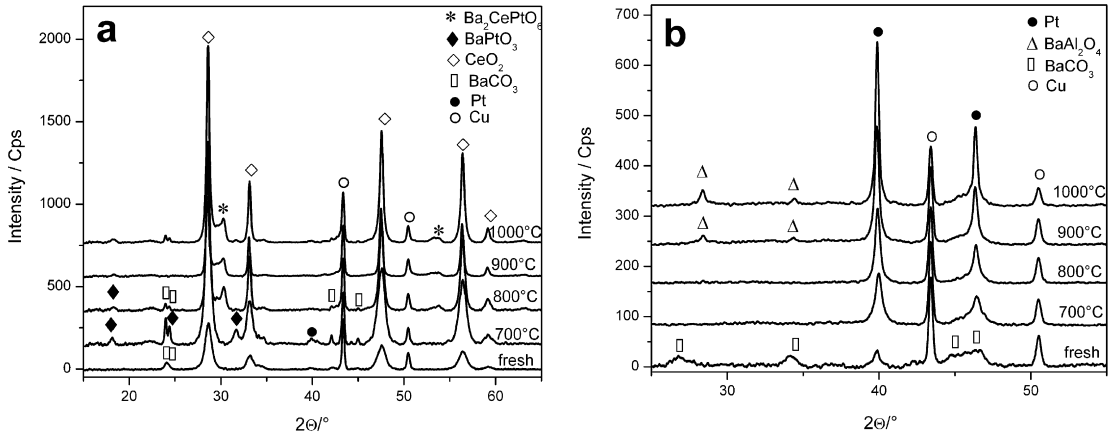

Fig. 5. XRD patterns recorded for 10-Pt/Ba/CeO_2 (a) and 10-Pt/Ba/Al_2O_3 (b) calcined for 12 h at different temperatures.

3.2.3. Low-loading samples 1-Pt/Ba/CeO_2 and 1-Pt/Ba/Al_2O_3

The significantly lower amount of Pt in commercial catalysts makes it impossible to apply the same characterization techniques, such as XRD or TA. Instead, XANES/EXAFS spectroscopy was used to study the local structure of Pt in the lower-loaded samples. The spectra were obtained in situ around the Pt L_3-edge (11.564 keV) in fluorescence mode. Fig. 6 shows the normalized XANES spectra recorded for 1-Pt/Ba/CeO_2 and 1-Pt/Ba/Al_2O_3 after calcination at 1000 °C for 12 h, in comparison with the spectrum of metallic Pt. The absorption intensity of the white line in the case of Pt L_3-edge reflects the vacancy in the 5d orbital of Pt atom (electron transition from 2p to 5d) and thus is related to the oxidation state. The strong white line intensity for the Pt/Ba/CeO_2 sample reveals a high oxidation state for the platinum constituent (Pt^{4+}), whereas for Pt/Ba/Al_2O_3, the intensity was the same as that of Pt foil, indicating that Pt was present mainly in a reduced state. For the ceria-supported samples, the EXAFS region was investigated to obtain information on the nearest neighbor atoms. The k^3-weighted Fourier-transformed EXAFS data (2.2–13.5 Å) of the 1-Pt/Ba/CeO_2 sample after calcinations in air at different temperatures between 600 and 1100 °C for 12 h are depicted in Fig. 7a. For comparison, EXAFS measurements (transmission mode) also were performed for the aged model systems: 10-Pt/Ba/CeO_2 samples and the mechanical mixtures of $BaCO_3$ and PtO_2. The corresponding Fourier-transformed EXAFS spectra of some selected samples are depicted in Fig. 7b, showing mainly a contribution at 1.7 Å (not corrected for phase shift) due to oxygen backscattering in the oxidized Pt–O clusters.

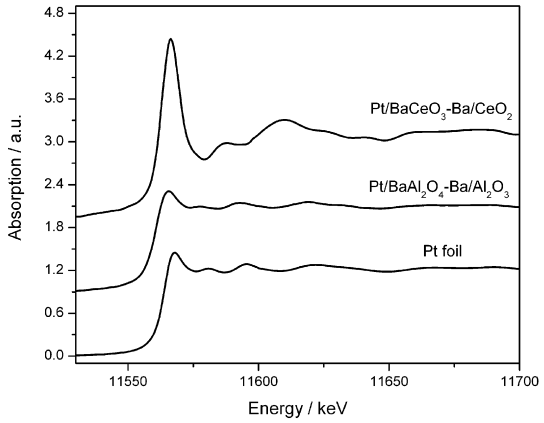

Fig. 6. Normalized XAS spectra measured at the Pt L_3-edge for 1-Pt/Ba/CeO_2 and 1-Pt/Ba/Al_2O_3 catalysts after aging at 1000 °C. For comparison the corresponding XAS spectrum of a Pt-foil is depicted.

To interpret the further backscattering peaks, theoretical spectra were calculated with the FEFF 6.0 code [36] using atomic coordinates of the $BaPtO_3$ [21,37] and Ba_2CePtO_6 [29] perovskite structures (generated with the ATOMS software tool). $BaPtO_3$ has a hexagonal multilayered perovskite structure, with Pt and Ba surrounded by 6 and 12 oxygen ions, respectively. The double-perovskite crystal structure of Ba_2CePtO_6, determined by Ouchetto et al. [29] from XRD measurements, contains octahedrally coordinated Ce and Pt over an ReO_3-type framework with Ba positioned in all cubic cavities.

For both supported systems (low- and high-Pt loaded), apart from the oxygen neighbor, the presence of a small amount of metallic platinum (Pt–Pt bond at 2.75 Å; see the reference spectrum in Fig. 7b) was observed between 600 and 900 °C. This probably resulted from decomposition of those PtO_2 particles that were not in contact with Ba species on CeO_2 surface after catalyst preparation. The rest of platinum remained in oxidized state also at 1000 °C. In the Fourier-transformed EXAFS spectrum of the 10-Pt/Ba/CeO_2 model catalyst after calcination at 700 °C, the peaks at 1.7 and 2.6 Å also can be assigned to the Pt–O and Pt–Pt bonds, respectively.

In both high- and low-loaded catalysts, calcined above 800 °C, further peaks were found at 3.6 and 4.2 Å, which can be attributed to the Ba and Ce atoms in the perovskite lattice of the Ba_2CePtO_6 in rather linear coordination within Pt–O–Ce. This contribution increased at 1000 °C, which is in line with the XRD results on the high-loaded model catalyst. A similarly strong contribution in Fourier-transformed EXAFS spectra was observed previously on formation of the $BaCeO_3$-perovskite [8].

Formation of the mixed oxides during aging of the 1-Pt/Ba/CeO_2 model catalyst also was confirmed by high-angle an-

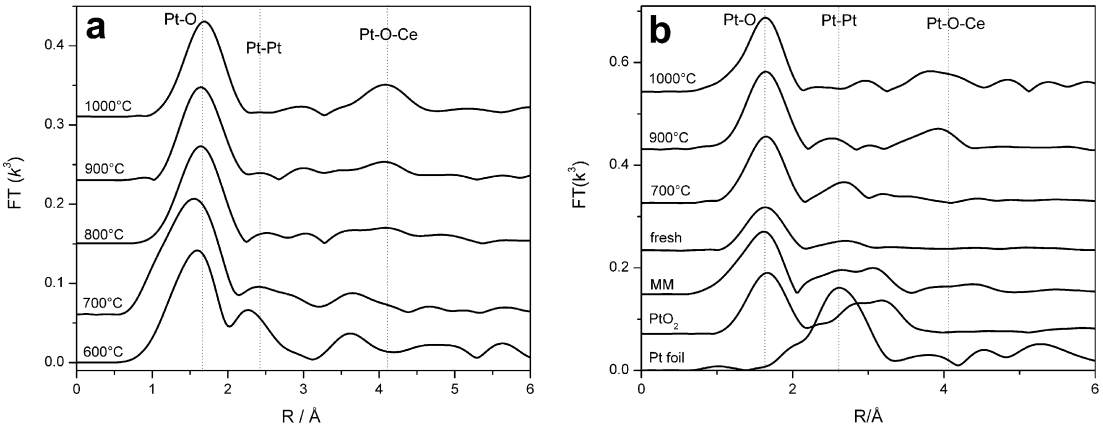

Fig. 7. Fourier-transformed EXAFS spectra (k^3-weighted) at the Pt L_3-edge of 1-Pt/Ba/CeO_2 (a) and of 10-Pt/Ba/CeO_2 (b) recorded in fluorescence and transmission mode, respectively, for the fresh and aged samples (calcinations in air at selected temperatures for 12 h); for comparison, the FT-EXAFS spectra of a Pt foil, PtO_2 and of the mechanical mixture of $BaCO_3$–PtO_2 (4:1) after calcination in air for 12 at 900 °C (denoted MM) are presented in (b).

nular dark field STEM (HAADF-STEM) combined with spot energy-dispersive X-ray spectroscopy analysis (EDXS). The investigations were performed with 1-Pt/Ba/CeO_2 calcined at 700 and 1000 °C, which should contain $BaPtO_3$ and Ba_2CePtO_6, respectively. The sample with high Pt loading calcined at the same temperatures for 12 h was used for comparison. EDX analysis of the low- and high-loaded Pt/Ba/CeO_2 samples revealed the presence of Ba and Pt species at the same locations corresponding to the presence of $BaPtO_3$ and Ba_2CePtO_6 (Figs. 8 and 9a), whereas for the 1-Pt/Ba/Al_2O_3 catalyst, the electron microscopy data collected after calcination in air revealed significant sintering only of Pt particles (Fig. 9b).

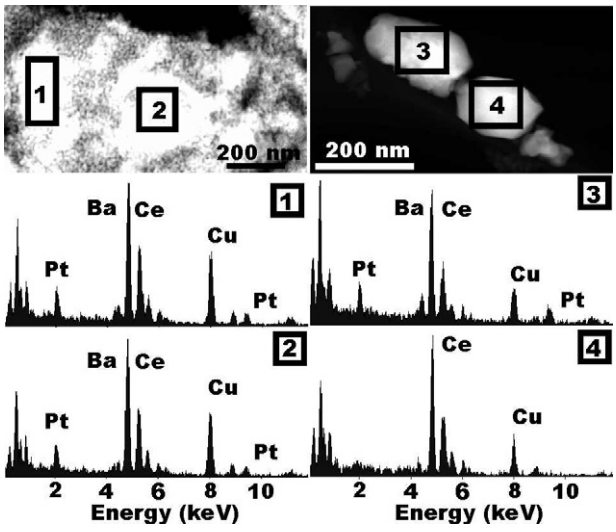

Fig. 8. STEM images of 10-Pt/Ba/CeO_2 calcined for 12 h at 700 and 1000 °C. The EDX spectra obtained from the outlined areas are shown below.

3.3. Stability of $BaPtO_3$ and Ba_2CePtO_6 in H_2 atmosphere

The reduction of the Ba–Pt mixed oxides prepared by calcination of mechanical mixtures of $BaCO_3$ and PtO_2 was investigated by temperature-programmed reduction (TPR) with 10 °C/min up to 500 °C under 10% H_2/He. $BaPtO_3$ and all $BaPtO_{3-x}$ were found to be unstable in the presence of H_2 at low temperature. $BaPtO_3$ formed in the mechanical mixture of $BaCO_3$ and PtO_2 (1:1 molar ratio) after calcination at 700 °C for 12 h began to reduce at ca. 105 °C. The XRD data revealed the formation of Pt and $Ba(OH)_2$ due to the reaction of freshly formed BaO with H_2O from the ambient atmosphere (data not shown). This observation is in line with the findings of Gallagher et al. [21] on the reduction of $BaPtO_3$ in pure H_2.

TPR measurements also were used to study the stability in hydrogen of $BaPtO_3$ and Ba_2CePtO_6 supported on CeO_2. The reduction was carried out with two samples containing $BaPtO_3$ (10-Pt/Ba/CeO_2 calcined at 700 °C) and Ba_2CePtO_6 (10-Pt/Ba/CeO_2 calcined at 1000 °C). The TG and DTG curves recorded during heating in 10% H_2 are depicted in Fig. 10a. The reduction of both perovskites occurred at 130–210 °C. The products of the reduction of $BaPtO_3$ were Pt and BaO (which in turn react further with H_2O or CO_2 from the ambient atmosphere), whereas Ba_2CePtO_6 was reduced to Pt, BaO, and $BaCeO_3$.

Complete recovery of the NO_x storage active components of thermally aged Pt/Ba/CeO_2 can be achieved using the reaction of $BaCeO_3$ with H_2O/NO_2 or CO_2 [8]. Fig. 10b shows the XRD patterns of 10-Pt/Ba/CeO_2 after calcination in air at 1000 °C for 12 h, followed by reduction in 10% H_2 during heating up to 300 °C and finally, after the decomposition of $BaCeO_3$ (formed during the reduction step) by reaction with CO_2 (heating up to

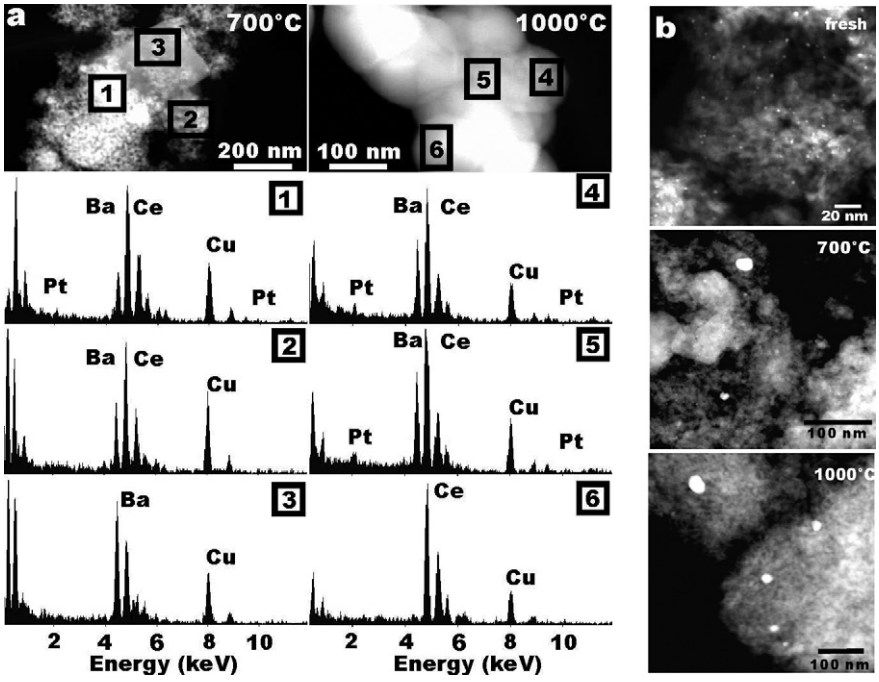

Fig. 9. STEM images of 1-Pt/Ba/CeO_2 calcined for 12 h at 700 and 1000 °C with the EDX spectra obtained from the outlined depicted below (a); STEM images of 1-Pt/Ba/Al_2O_3 fresh and calcined in air for 12 h at 700 and 1000 °C (b).

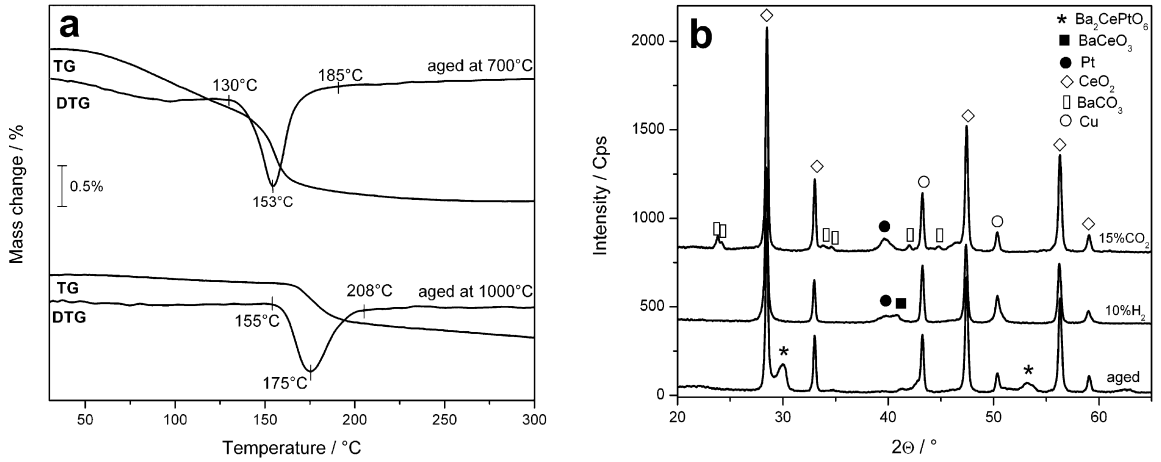

Fig. 10. TG and DTG curves (a) recorded during reduction of 10-Pt/Ba/CeO_2 after calcination at 700 °C (12 h, mainly containing $BaPtO_3$) and calcination at 1000 °C (12 h, mainly Ba_2CePtO_6 and XRD patterns (b) of the same sample aged at 1000 °C, after reduction in 10% H_2/He and after decomposition of $BaCeO_3$ in 15% CO_2/He.

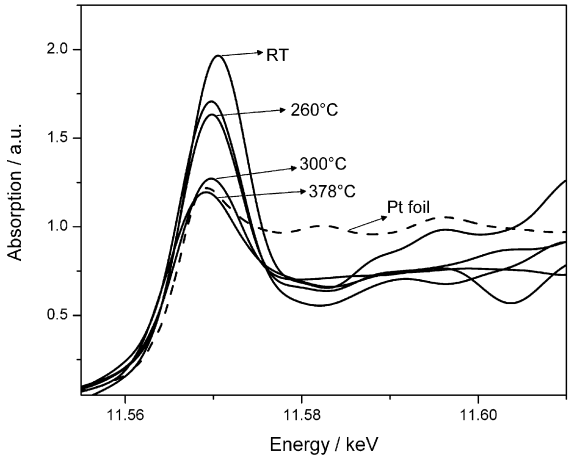

Fig. 11. Normalized XAS spectra collected at the Pt L_3-edge of the aged 1-Pt/Ba/CeO_2 catalyst (in air, 1000 °C, 12 h) during reduction in 5% H_2/He.

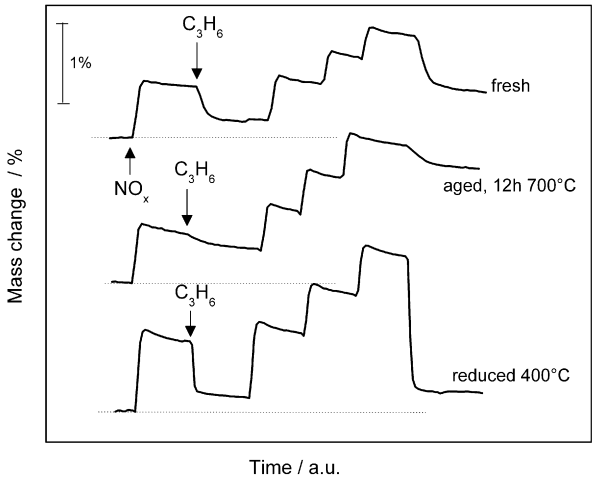

Fig. 12. Mass changes indicating NO_x storage (NO, O_2 pulses) and reduction (C_3H_6 pulses) activity for the fresh, aged (700 °C in air, 12 h) and reactivated (H_2 pulses at 400 °C) 1-Pt/Ba/CeO_2 catalyst

900 °C in 15% CO_2/He). The sample obtained after both treatments contained only $BaCO_3$ and metallic Pt (the active NO_x storage and reduction components).

The reduction of Ba_2CePtO_6 in H_2-containing atmosphere also was investigated for the 1-Pt/Ba/CeO_2 sample after aging in air at 1000 °C for 12 h. In this case, in situ Pt L_3 XANES measurements were performed during heating at 5 °C/min in 5% H_2/He. Fig. 11 shows the XANES region recorded at different temperatures during reduction. The decrease in the white line corresponds to the reduction of Pt^{4+} to Pt^0. The formation of the metallic Pt occurs between 250 and 350 °C.

3.4. The effect of $BaPtO_3$ formation on NO_x storage-reduction activity of Pt/Ba/CeO_2

NO_x storage-reduction activity of the catalysts was investigated at 300 °C by the PulseTA method [25] for the fresh 1-Pt/Ba/CeO_2, the corresponding sample calcined at 700 °C for 12 h, and the calcined sample after reduction (four 1-mL pulses of H_2 at 400 °C). Before each experiment, the sample was heated up to 500 °C in He to remove all physisorbed species. Alternating 1-mL NO and 1-mL O_2 pulses (2 pulses of NO and 3 pulses of oxygen) where injected into the He carrier gas every 15 min to simulate the NO_x-trapping process. Catalyst regeneration was done with 1-mL pulses of C_3H_6 (single pulse). The TG curves recorded during these NSR experiments are shown in Fig. 12. The mass changes observed during storage represent the sum of two effects: $Ba(NO_3)_2$ formation and $BaCO_3$ decomposition during NO/O_2 pulses. The mass loss occurring during reduction with propene represents the opposite reactions. These findings demonstrate similar storage capacity for all compared samples. The storage activity observed for even the $BaPtO_3$-containing sample (the 1-Pt/Ba/CeO_2 sample calcined for 12 h at 700 °C), in which Pt was in an oxidized state, can be explained by the high temporary concentration of NO (ca. 10,000 ppm immediately after injection), which shifts the equilibrium of NO oxidation toward NO_2 formation. This explains why in the absence of Pt particles, the catalyst has still high activity in NO_x storage; the very small amount of metal-

lic Pt uncovered in the Fourier-transformed EXAFS spectra of the aged catalyst would not cause the same NO_x storage capacity as observed in the fresh catalyst. On the other hand, during catalyst regeneration, in which the presence of Pt particles is required for C_3H_6 cracking, the effect of thermal aging can be distinctly observed. In the aged material, Pt was present mainly as $BaPtO_3$, which is significantly less active in the regeneration process. The reduction of $BaPtO_3$ by hydrogen pulses at 400 °C led to the formation of metallic Pt, which is active for C_3H_6 cracking, and thus to the recovery of the NO_x reduction activity (Fig. 12). The obvious improvement in the overall NO_x storage-reduction behavior by formation of the Pt–Ba composites at 700 °C and their subsequent reduction is interesting and presently under further investigation.

4. Discussion

The present study has given new insight into the fate of Pt during thermal aging of a NO_x storage catalyst. Systematic studies of possible Pt composite formation under oxidizing atmosphere were performed using a series of different systems: mechanical mixtures of $BaCO_3$–PtO_2, high-loaded Pt/Ba/CeO_2 and Pt/Ba/Al_2O_3 model catalysts, and low-loaded Pt NSR catalysts. Investigation of high-loaded Pt samples allows comparison with the literature data and the use of a broader spectrum of analytical techniques. In contrast, the study of low-loaded samples, even if performed under idealized conditions, may give an indication for interpretation of the phenomena occurring in the commonly used catalytic systems.

In a mechanical mixture of $BaCO_3$ and PtO_2, the formation of $BaPtO_3$ as a first Ba–Pt mixed oxide was observed at relatively low temperature (600 °C); see Figs. 2a and 2b. These findings demonstrate that the molar ratio between the two components does not influence the reaction stoichiometry. At higher temperatures, the formation of $BaPtO_{2.38}$ by decomposition of $BaPtO_3$ was observed. Mixed Ba–Pt oxides with higher Ba content, reported in literature [18,22,23], were not observed during this study, probably due to the different conditions. The formation of $BaPtO_3$ at 600–700 °C in the high-loaded 10-Pt/Ba/CeO_2 sample was observed by XRD, XAS, and electron microscopy. Above 800 °C, Ba-containing phases also reacted with CeO_2 to $BaCeO_3$ [8]. Some of the $BaCeO_3$ immediately reacted further with $BaPtO_3$ and formed Ba_2CePtO_6 (Fig. 5a), which decomposed at 1050 °C into $BaCeO_3$ and Pt. The formation of $BaPtO_3$ and Ba_2CePtO_6 perovskites in the low-loaded Pt/Ba/CeO_2 sample was also indicated by XAS and electron microscopy measurements. Analysis of the Fourier-transformed EXAFS spectra revealed the formation of crystalline Pt-composite phases above 800 °C. In contrast to the high-loaded Pt sample, in the 1-Pt/Ba/CeO_2 material, Ba_2CePtO_6 was stable even at 1100 °C; the Fourier-transformed EXAFS spectrum of 1-Pt/Ba/CeO_2 after calcinations at 1100 °C revealed an oxidized state for Pt.

For the Pt/Ba/Al_2O_3 systems, no mixed Pt–Ba oxides were found as in the mechanical mixtures of $BaCO_3$ and PtO_2. Instead, the behavior of Pt corresponded closely to the results of previous studies on sintering of Pt particles in an oxidizing atmosphere on Al_2O_3 with or without Ba in the system [10,11,38,39].

At first glance, the absence of $BaPtO_3$ formation in Al_2O_3-supported catalysts is surprising, considering the behavior of $BaCO_3$ toward PtO_2 in a mechanical mixture. A closer examination of both alumina- and ceria-containing systems suggests some possible explanations, however. The good dispersion of Pt on the CeO_2 support and the decoration of the noble metal particles with CeO_2 may be caused by the well-known strong metal–support interaction (SMSI) typically observed under reducing conditions [40–42]. In fact, more recent studies have revealed the formation of strong Pt–CeO_2 interactions also under oxidizing conditions [43,44], which keep Pt particles highly dispersed even at high temperatures (up to 800 °C). Thus, due to higher dispersion, PtO_x may react more readily with Ba-containing phases. In contrast, on Al_2O_3, due to the absence of a strong interaction with the support, the formation and the sintering of metallic Pt occur faster and at lower temperatures [44].

Moreover, the interaction of Ba-containing species with the Al_2O_3 and CeO_2 supports differs, which may play an important role. For alumina, it is known that Ba compounds can act as dopants to suppress the γ- to α-Al_2O_3 phase transition and prevent a decrease in surface area and the sintering of noble metal species [33,35,45,46]. The higher affinity of BaO toward Al_2O_3 in comparison with Pt leads to the possible formation of –Ba–O–Al– surface bonds and, at higher temperatures, to formation of crystalline $BaAl_2O_4$ and $BaAl_{12}O_{19}$. Formation of these phases seems to be the cause of Al_2O_3 stabilization. Such intimate contact between BaO and Al_2O_3 and the formation of monolayer of Ba-containing phases also has been suggested for Pt/Ba/Al_2O_3 NO_x storage-reduction catalysts [28]; this indicates that the strong interaction of Ba species with the Al_2O_3 surface hampers the formation of Ba–Pt mixed oxides.

In contrast to Al_2O_3, due to the higher basicity of CeO_2 [47], the interaction of BaO with the support is weaker in Pt/Ba/CeO_2. Thus the BaO, already present in the system or resulting from $BaCO_3$ decomposition can react with the Pt constituent and, at higher temperature, with CeO_2 as well.

The sintering of Pt and the formation Pt composites may have a detrimental effect on the NO_x storage-reduction properties of both Pt/Ba/Al_2O_3 and Pt/Ba/CeO_2 catalysts; therefore, their reactivation is an important aspect. For the Pt/Ba/Al_2O_3 catalyst, sintering of Pt particles caused by long exposure to high temperatures (above 750°) in oxidizing or reducing environments has been reported to negatively affect both the storage and reduction properties [10,48,49]. Thus, redispersion of Pt particles is important; however, strategies for this, such as oxychlorination [48] or reoxidation of Pt metallic particles between 500 and 600 °C [50], are still not ideal and are difficult to apply in practice.

In contrast, in the aged Pt/Ba/CeO_2 catalyst, the formation of $BaPtO_3$ and Ba_2CePtO_6 mixed oxides was observed instead of Pt sintering. Although this keeps the Pt in a finely distributed state, it nevertheless leads to a loss of the NSR activity. Interestingly, we observed that the activity of the Pt can be recovered by the reduction of the aged catalyst with H_2 at relatively low

temperature. This reduction was observed by TA and XRD for the high-loading Pt samples (Figs. 10a and 10b) and by in situ EXAFS for the low-loading 1-Pt/Ba/CeO_2 catalyst (Fig. 11). The reduction products, obtained in 10% H_2 at ca. 160 °C, were Pt and BaO or Pt and $BaCeO_3$, depending on the previous aging temperature.

The beneficial effect of the reducing treatment was confirmed by monitoring the NO_x storage-reduction activity of an aged 1-Pt/Ba/CeO_2 catalyst (12 h at 700 °C in air). In this catalyst, all platinum was present in the form of $BaPtO_3$. NO_x storage-reduction experiments performed for the fresh, aged, and reactivated catalysts demonstrated a loss of NSR activity after aging and recovery of activity after catalyst reactivation by reduction in hydrogen (Fig. 12).

Exposure of Pt/Ba/CeO_2 catalysts to temperatures above 800 °C led to the formation of two composites, Ba_2CePtO_6 and $BaCeO_3$. Fortunately, the Ba_2CePtO_6 double perovskite also can be reduced by H_2. Thus, highly dispersed metallic Pt particles can be obtained by reduction of the aged catalyst at relatively low temperature. $BaCeO_3$, the second product obtained by aging or reduction of Ba_2CePtO_6, also can be decomposed even under certain engine operating conditions, as we have demonstrated in a previous study [51]. Thus, all components present in fresh Pt/Ba/CeO_2 catalysts can be restored after aging by different treatments. However, the possibility that part of the active components may be encapsulated in the CeO_2 lattice cannot be excluded.

The results demonstrate that platinum behaves differently during the aging of ceria- or alumina-supported catalysts and that different reactivation procedures are required. In this regard, selecting the support for the NO_x storage-reduction catalysts must take into account not only surface area and platinum and barium dispersion, but also the new findings concerning $BaPtO_3$ and Ba_2CePtO_6 formation and possible reactivation of the aged cerium oxide-supported catalysts. Further studies are underway on the roles of the reaction and interaction of Pt with Ba species and ceria, as well as their effect during preparation.

5. Conclusion

The present study demonstrates that Pt behaves significantly differently in the thermal aging of Pt/Ba/CeO_2 and Pt/Ba/Al_2O_3 catalysts. On CeO_2-supported catalysts, the behavior of Pt resembles that in a mechanical mixture of $BaCO_3$ and PtO_2, with $BaPtO_3$ formed at relatively low temperature (600–700 °C). Above 800 °C, $BaPtO_3$ reacts further with $BaCeO_3$ (resulting from the reaction between Ba-containing species and CeO_2) to form a double perovskite Ba_2CePtO_6. Both perovskites, which keep the Pt well dispersed, can be reduced with H_2 at relatively low temperatures, thus restoring the catalytically active Pt species. Investigation of the NO_x storage and reduction activity of the fresh, aged, and reduced ceria-supported catalyst confirmed the recovery of the activity and the efficiency of the reduction treatment. In contrast, sintering only of Pt particles and no Pt–Ba oxides could be observed in both high- and low-loaded Pt/Ba/Al_2O_3 catalysts. Thus, during aging, not only barium–ceria and barium–alumina composite formation, but also the fate of platinum differs significantly. This demands different reactivation procedures for the two catalyst systems and has considerable implications for the choice of the proper support material for a particular application.

Acknowledgments

M.C. gratefully acknowledges financial support by Umicore and beamtime allocations at HASYLAB (DESY, Hamburg). The authors thank Dr. Frank Krumeich (Electron Microscopy Center of ETH Zurich) for performing the electron microscopy investigations; the Swiss Norwegian Beamline (SNBL at ESRF, Grenoble) for beamtime for in situ fluorescence XAS measurements; and Edmund Welter and Adam Webb at beamline X1 at HASYLAB, Hermann Emerich and Wouter van Beek at SNBL, as well as Peter Haider, Bertram Kimmerle, Stefan Hannemann, Matteo Caravati, and Fabian Jutz (ETH Zürich) for the support during our EXAFS measurements.

References

[1] K.-H. Glück, U. Göbel, H. Hahn, J. Höhne, R. Krebs, T. Kreuzer, E. Pott, MTZ 61 (2000) 6.
[2] R. Krebs, L. Spiegel, B. Stiebels, in: 8. Aachener Kolloquium Fahrzeug- und Motorentechnik, Aachen, 1999.
[3] W. Bögner, M. Krämer, B. Krutzsch, S. Pischinger, D. Voigtländer, G. Wenninger, F. Wirbeleit, M.S. Brogan, Appl. Catal. B 7 (1995) 153.
[4] N. Miyoshi, S. Matsumoto, K. Katoh, T. Tanaka, J. Harada, N. Takahashi, K. Yokota, M. Sugiura, K. Kasahara, SAE Tech. paper 950809 (1995); N. Takahashi, H. Shinjoh, T. Iijima, T. Suzuki, K. Yamazaki, K. Yokota, H. Suzuki, N. Miyoshi, S. Matsumoto, T. Tanizawa, T. Tanaka, S. Tateishi, K. Kasahara, Catal. Today 27 (1996) 63.
[5] S. Matsumoto, Cattech 4 (2000) 102.
[6] E. Fridell, H. Persson, B. Westerberg, L. Olsson, M. Skoglundh, Catal. Lett. 66 (2000) 71.
[7] P. Engstrom, A. Amberntsson, M. Skoglundh, E. Fridell, G. Smedler, Appl. Catal. B 22 (1999) 241.
[8] M. Casapu, J.-D. Grunwaldt, M. Maciejewski, M. Wittrock, U. Göbel, A. Baiker, Appl. Catal. B 63 (2005) 232.
[9] B.-H. Jang, T.-H. Yeon, H.-S. Han, Y.-K. Park, J.-E. Yie, Catal. Lett. 77 (2001) 1.
[10] G.W. Graham, H.-W. Jen, W. Chun, H.P. Sun, X.Q. Pan, R.W. McCabe, Catal. Lett. 93 (2004) 129.
[11] D. Uy, A.E. O'Neill, J. Li, W.L.H. Watkins, Catal. Lett. 95 (2004) 191.
[12] G.W. Graham, H.-W. Jen, W. Chun, R.W. McCabe, J. Catal. 182 (1999) 228.
[13] G.W. Graham, A.N. Shigapov, Catal. Lett. 81 (2002) 253.
[14] C.H. Bartholomew, Appl. Catal. A 212 (2001) 17.
[15] N. Fekete, R. Kemmler, D. Voigtländer, B. Krutzsch, E. Zimmer, G. Wenninger, W. Strehlau, J. Tillaart, J. Leyrer, E.S. Lox, W. Müller, SAE Tech. paper 970746 (1997).
[16] H.C. Yao, S. Japar, M. Shelef, J. Catal. 50 (1977) 407.
[17] M. Hatano, Catal. Surv. Asia 7 (2003) 281.
[18] A.P. Wilkinson, A.K. Cheetham, Acta Crystallogr. C 45 (1989) 1672.
[19] S.J. Schneider, C.L. McDaniel, J. Am. Ceram. Soc. 52 (1969) 518.
[20] J.J. Randall, W. Roland, J. Am. Chem. Soc. 81 (1959) 2629.
[21] P.K. Gallagher, D.W. Johnson, E.M. Vogel, G.K. Wertheim, F.J. Schnettler, J. Solid State Chem. 21 (1977) 277.
[22] W.O. Statton, J. Chem. Phys. 19 (1951) 33.
[23] P.S. Haradem, B.L. Chamberland, L. Katz, A. Gleizes, J. Solid State Chem. 21 (1977) 217.
[24] J. Vacinova, J.L. Hodeau, J. Solid State Chem. 140 (1998) 201.
[25] M. Maciejewski, C.A. Muller, R. Tschan, W.D. Emmerich, A. Baiker, Thermochim. Acta 295 (1997) 167.

[26] S. Hannemann, M. Casapu, J.-D. Grunwaldt, P. Haider, P. Trüssel, A. Baiker, E. Welter, J. Synch. Rad. 14 (2007) 345.
[27] T. Ressler, J. Synch. Rad. 5 (1998) 118.
[28] M. Piacentini, M. Maciejewski, A. Baiker, Appl. Catal. B 59 (2005) 187.
[29] K. Ouchetto, F. Archaimbault, A. Pineau, J. Choisnet, J. Mater. Sci. Lett. 10 (1991) 1277.
[30] M. Piacentini, M. Maciejewski, A. Baiker, Appl. Catal. B 60 (2005) 265.
[31] M.F.L. Johnson, J. Catal. 123 (1990) 245.
[32] H.K. Kang, S.S. Park, M.M. Son, H.S. Lee, H.C. Park, Br. Ceram. Trans. 99 (2000) 26.
[33] M. Machida, K. Eguchi, H. Arai, J. Catal. 103 (1987) 385.
[34] V. Labalme, N. Guilhaume, E. Garbowski, M. Primet, Catal. Lett. 64 (1998) 207.
[35] V. Labalme, E. Garbowski, N. Guilhaume, M. Primet, Appl. Catal. A 138 (1996) 93.
[36] B. Ravel, J. Synch. Rad. 8 (2001) 314.
[37] J. Johnson Jr., P.K. Gallagher, G.K. Wertheim, E.M. Vogel, J. Catal. 48 (1977) 87.
[38] W.G. Rothschild, H.C. Yao, H.K. Plummer, Langmuir 2 (1986) 588.
[39] D.D. Beck, C.J. Carr, J. Catal. 110 (1988) 285.
[40] A. Trovarelli (Ed.), Catalysis by Ceria and Related Materials, Imperial College Press, London, 2002.
[41] X. Tang, B. Zhang, Y. Li, Y. Xu, Q. Xin, W. Shen, Catal. Lett. 97 (2004) 163.
[42] M. Abid, V. Paul-Boncour, R. Touroude, Appl. Catal. A 297 (2006) 48.
[43] S. Hosokawa, M. Taniguchi, K. Utani, H. Kanai, S. Imamura, Appl. Catal. A 289 (2005) 115.
[44] Y. Nagai, T. Hirabayashi, K. Dohmae, N. Takagi, T. Minami, H. Shinjoh, S. Matsumoto, J. Catal. 242 (2006) 103.
[45] K. Okada, A. Hattori, T. Taniguchi, A. Nukui, R.N. Das, J. Am. Ceram. Soc. 83 (2000) 928.
[46] C.H. Bartholomew, Stud. Surf. Sci. Catal. 111 (1997) 585.
[47] D. Martin, D. Duprez, J. Phys. Chem. 100 (1996) 9429.
[48] W. Epling, L. Campbell, A. Yezerets, N. Currier, J. Parks, Catal. Rev. 46 (2004) 163.
[49] D.H. Kim, Y.-H. Chin, G.G. Muntean, A. Yezerets, N.W. Currier, W.S. Epling, H.-Y. Chen, H. Hess, C.H.F. Peden, Ind. Eng. Chem. Res. 45 (2006) 8815.
[50] J.E. Stulga, R. Mariscal, J.A. Tien, Appl. Catal. 59 (2005) 59.
[51] M. Casapu, J.-D. Grunwaldt, M. Maciejewski, A. Baiker, M. Wittrock, U. Göbel, S. Eckhoff, Top. Catal. 42–43 (2007) 3.